

**Sulfide mineral reaction rates determined from measurements of
reaction product coating thickness: Method evaluation and potential
applications**

November, 2017

Zach Wenz
Steven Koski

Minnesota Department of Natural Resources
Lands and Minerals Division
500 Lafayette Road
Saint Paul, MN 55155-4045

Table of Contents

List of Tables	i
List of Figures	i
Executive Summary.....	ii
1. Introduction	1
2. Methods.....	2
2.1 Sample Preparation	3
2.2 Reflected Light Microscopy.....	3
2.3 Theoretical Basis of Calculation	4
2.4 Rate Calculation Procedure.....	5
3. Results	7
3.1 Petrography	7
3.2 Microscope Measurements and Apparent Rate Calculations	8
3.3 Sensitivity Analysis of the Apparent Rate Calculation	8
3.4 Comparison to Available Reaction Rate Data	9
4. Conclusions	10
5. Acknowledgements.....	11
6. References	12
Tables	14
Figures.....	18

LIST OF TABLES

Table 1. Sulfide grain coating average thickness measurements and corresponding apparent reaction rates.	14
Table 2. Mineral molar volumes	15
Table 3 Bimodal sulfide grains with associated apparent reaction rates	15
Table 4. BET and geometric surface area conversion data	15
Table 5. Ferric iron geochemical model input and output data	17
Table 6. Pore water pH geochemical model	17

LIST OF FIGURES

Figure 1. Illustration of cross-sections through the center of a sulfide grain with a uniform oxidation reaction product coating..	18
Figure 2. Schematic illustrating the relationship between coating thickness from measured grains and the particle lifetime conceptualized counterpart.	19
Figures 3A and 3B. Images of the two bimodal sulfide mineral grains observed.....	20
Figure 4. Sulfide mineral oxidation rate plot illustrating chalcopyrite and pyrrhotite rate laws and rate data.....	21
Figure 5. Pyrite oxidation rate laws from Williamson and Rimstidt (1994) illustrating the change in pyrite oxidation rate with pH and oxidant type	22

EXECUTIVE SUMMARY

Accurately accounting for sulfide mineral oxidation rates is of primary importance for understanding the short and long term reactivity of mine wastes (e.g. waste rock, tailings, and overburden). Typical mine waste characterization studies employ laboratory and field leach tests (e.g., humidity cell tests) to quantify solute (e.g., sulfate, copper, nickel, etc.) release from mine wastes. In turn, the solute release data from leach tests is routinely used in water quality models for mining influenced waters. Despite this common practice, there has been a limited amount of work focused on quantifying the various hydrogeochemical processes under which these laboratory and field tests operate. These limitations can lead to large uncertainties in water quality model results and may result in improper use of solute release data for addressing the potential impacts of mine wastes to the environment.

In this method evaluation study, sulfide mineral reaction rates were calculated from reaction product coating thicknesses determined from microscope examination of weathered material from laboratory rock weathering experiments (e.g., humidity cell). Oxidation coating thickness measurements on pyrite grains from Minnesota taconite tailing basins, collected from a previous study, were also used to assess whether or not this explorative technique is applicable for natural settings. The study results indicated that this relatively simple and straightforward technique has the potential to accurately calculate the reaction rates of sulfide minerals from both laboratory experiments and naturally weathered mine wastes. Importantly, this study focused on calculating the rate of individual mineral reactions, whereas solute release data typically collected from laboratory weathering tests is a combined reaction signal from multiple unconstrained mineral reactions. Comparison of the sulfide reaction rates calculated in this study to sulfide mineral reaction rate laws from published literature values showed reasonable agreement, indicating this approach may be useful for quickly and accurately understanding the sulfide oxidation reactions occurring in field and laboratory settings. However, as an initial evaluation of the technique, the sulfide oxidation rates calculated in this report only serve as examples of the method approach and should not be used for predictive purposes. Further refinement and evaluation methods are identified that would improve the accuracy and reduce the uncertainty of the reaction rate values.

1. INTRODUCTION

The composition of leachate from chemically weathering rocks is primarily a function of rock mineralogy. Most igneous and metamorphic rocks consist of four basic groups of minerals including silicates, oxides, carbonates, and sulfides. Silicate minerals are by far the most abundant, typically accounting for about 95 volume percent of a rock. The remaining 5 volume percent is split among the other three basic mineral groups typically decreasing in amount in the order of oxides, carbonates, and sulfides. For Earth surface weathering processes, common oxides (e.g., magnetite and ilmenite) are essentially inert and the majority of silicate minerals react much slower than carbonates and sulfides. Due to the substantial difference in mineral reaction rates, where present, carbonate and sulfide mineral reactions predominantly control the chemistry of rock leachates. During mildly acidic surface weathering processes, silicate minerals typically incongruently dissolve generating both aqueous and solid phase (e.g., secondary minerals or amorphous compounds) reaction products. In strongly acidic environments (pH less than about 4) even the most refractory secondary mineral phases (e.g., Al-hydroxides) are soluble and stoichiometric dissolution of most minerals will occur. In contrast to silicates, most carbonate minerals readily dissolve under mildly acidic conditions (e.g., natural precipitation with a pH of about 5.5). Whereas silicates and carbonate reactions are typically dissolution or incongruent dissolution involving an acid, sulfide mineral reactions occur as either a dissolution type or oxidation type depending on the governing chemical system. Oxidation reactions include an oxidant (an electron donor) and a reductant (an electron receptor). The primary oxidants involved in sulfide oxidation reactions are water, dissolved oxygen, and ferric iron. Sulfide minerals are commonly classified as acid-insoluble (e.g., pyrite) or acid-soluble (e.g., chalcopyrite and pyrrhotite) based on reaction behavior. Acid-insoluble sulfides are relatively insoluble in acidic solutions, but are very reactive in oxic acidic solutions and moderately reactive in oxic and mildly to non-acidic solutions. Acid-soluble sulfides dissolve readily in strongly acidic solutions and are also reactive in less acidic oxic solutions. The oxidative reaction rate of iron sulfide minerals (e.g., pyrite and pyrrhotite) in mine wastes are of similar magnitude as the dissolution rate of the fastest reacting carbonates. Sulfide oxidation is the driving reaction responsible for the generation of acid and release of sulfate and metals during rock weathering processes. Specifically, it is the oxidation of iron-bearing sulfides that contribute sulfuric acid to the rock weathering environment that leads to increased rates of carbonate and silicate dissolution. In the absence of iron sulfide minerals, most igneous and metamorphic rocks weather at much slower rates because the only source of acidity is weak carbonic acid derived from atmospheric carbon dioxide.

Mineral reaction rates, such as sulfide oxidation, are commonly calculated using batch flow reactors or similar experimental techniques (Brantley and Conrad, 2008). These reaction rate determination experiments relate the reaction product aqueous concentration change over time to a reactant mineral surface area. The surface area is commonly measured based on the average geometric area or that determined by gas sorption techniques (e.g., the BET method (Brunauer et al., 1938)), thus these rates are commonly referred to as 'surface area normalized' reaction rates. The surface area normalized oxidation rates of iron-bearing sulfides at Earth surface conditions have only been investigated for pyrite and pyrrhotite. Pyrite has received the most attention largely due to being recognized as the primary source of acid mine drainage for coal spoils and mine wastes worldwide. The dependence of the pyrite reaction rate on pH and ferric iron and oxygen concentration have been measured over a range of chemical environments (i.e., different pH, dissolved oxygen and iron concentrations) encompassing most earth surface conditions (e.g., Williamson and Rimstidt, 1994; and McKibben and Barnes, 1986). The multiple reaction steps involved in the overall pyrite oxidation reaction have been fully described based on the electrochemistry of the reaction steps (Holmes and Crundwell, 2000). Oxidation rates for pyrrhotite

have also been assessed, although over a smaller range of earth surface conditions (e.g., Chirita and Rimstidt, 2014; Janzen et al., 2000; and Nicholson and Scharer 1994). The next most studied iron-bearing sulfide oxidation rate is chalcopyrite. Multiple studies have measured the oxidation rate of chalcopyrite under acidic conditions (for pH values less than about 3) characterizing the rate dependence to ferric iron and oxygen concentrations. These studies were evaluated and combined to develop a set of chalcopyrite reaction rate laws for strongly acidic conditions (Kimball et al., 2010). The oxidation rates of other sulfides commonly found in Minnesota rocks, such as cubanite and pentlandite, have not been measured by standard batch flow reactors or other techniques to the authors' knowledge.

Field observations and various microanalysis techniques of different mine wastes have allowed qualitative ranking of the relative magnitude of reactivity for most common sulfides. The observations for ranking were largely based on the extent of oxidized coatings on the sulfide minerals at macro- and micro-scale. This qualitative reactivity order is pyrrhotite > pyrite > chalcopyrite (see Plumlee, 1999; and Jambor, 1994 and references within). Pentlandite has been observed to oxidize in tailing impoundments (Jambor, 1994), but the relative reactivity of pentlandite has not been incorporated into any lists. Although cubanite likely occurs in many mine wastes, no information is available regarding the relative rate of cubanite oxidation.

In summary, of the primary sulfides occurring in iron or copper-nickel deposits (i.e., pyrite, pyrrhotite, cubanite, chalcopyrite, and pentlandite) in the State of Minnesota, only pyrite has a well-defined reaction rate law for chemical conditions corresponding to Earth surface weathering conditions. Oxidation reaction rates for pyrrhotite cover a smaller range of conditions and the various reaction mechanisms and pathways involved are not entirely defined. Recent mineralogical investigations have indicated that the occurrence of Cu- and Fe-bearing sulfides in waste rock associated with copper-nickel deposits may be more prevalent than previously believed. Considering the substantial Cu-Ni resources in Minnesota more specific information regarding the relative reaction rates of the Cu- or Ni- and Fe-bearing sulfides is needed. This information would provide a foundation from which questions regarding the short and long term reactivity of mine wastes can be addressed. First, this information would enable more accurate interpretation of time series data collected from standard laboratory rock weathering experiments (i.e., kinetic tests, such as humidity cells) used in environmental review and mine permitting processes. Second, the specific reactions (e.g., oxidation, sorption, etc.) responsible for releasing metals and sulfate from mine wastes hosting multiple types of sulfides can be better understood by learning the relative rates of reaction among the sulfide minerals. The objective of this study is to assess whether or not sulfide oxidation rates can be determined from microscopic examination of reacted sulfide grains from natural and synthetic rock weathering environments such as tailing basins and humidity cell tests, respectively.

2. METHODS

This evaluation focused on rock material extracted from kinetic tests colloquially referred to as the 'particle size experiment' (Wenz et al., 2013, and Lapakko et al., 2006). The particle size experiment is a rock weathering test designed to evaluate the relationship between bulk reactivity and rock particle size. The particle size experiment samples consist of a series of different rock particle size fractions of crushed, sulfide-bearing, Duluth Complex norite that were subjected to a weekly rinsing procedure similar to that for standard humidity cells (e.g., ASTM D5744). The samples selected for inspection are from the < 0.053, 0.053-0.149 and 0.149-0.5 micrometer (um) size fractions of the particle size experiment. A single Duluth Complex sample from the colloquially named 'BLM experiment' was also used in the study. The BLM experiment consisted of a set of humidity cell tests for a variety of different rock types and testing protocols (Lapakko, 1999). Leachate pH of the selected samples from both of these experiments generally

ranged from about 4 to 6 although the samples from the two smallest size ranges had leachate pH values up to about 6.5 after approximately 700 weeks of reaction.

2.1 Sample Preparation

A few grams of weathered rock from previously discontinued kinetic tests were placed in silicone molds. The molds were placed in an air tight desiccator and a vacuum pump was used to achieve a 25 mm Hg vacuum. A very low viscosity epoxy (EPO-TEK 301-1) was dispensed over the top of the samples. After the samples were entirely covered by epoxy, to inhibit air returning to the evacuated pore spaces, an attached valve on the desiccator was opened allowing atmospheric pressure into the chamber forcing the low viscosity epoxy into the evacuated pores. This technique wholly imbeds all the rock particles and ensures the original near surface microstructures are maintained during the grinding and polishing steps of preparing a sample for reflected light microscopy. The epoxy embedded samples were oven cured at a temperature of about 65 °C. This temperature ensures a hard cure with very limited to no shrinkage. After curing, the epoxy embedded samples were ground and polished to a surface relief of 1 μm .

The same epoxy embedding technique was used for the 'BLM experiment' humidity cell sample. The large volume of epoxy required to encase the entire contents of the humidity cell generated sufficient heat for an adequate cure. Once the epoxy cured, the embedded humidity cell was sectioned to make a 2×3 inch billet. The billet was sent to National Petrographic to have a large polished thin section made. The thin section covers the entire height and center to edge of the rock material that was in the humidity cell.

2.2 Reflected Light Microscopy

Reflected light microscopy was performed with a Carl Zeiss Universal Polarizing Microscope equipped for transmitted and reflected light. The microscope was outfitted with an Optixcam Summit Series 5 megapixel digital camera. Standard reflected light microscopy techniques were used to observe the reflected light properties of the sulfide minerals and coating materials in the polished mounts and thin section. The petrographic work included mineral identification, measurement of sulfide grain size and coating thickness, and grain and coating morphology descriptions. Measurements of grain size and coating thicknesses were performed using ISCapture software. Sulfide mineral type determinations made with the Carl Zeiss microscope were reevaluated using an Olympus BX-5 microscope at the Natural Resources Research Institute (NRRI) in Duluth Minnesota. The BX-5 microscope enhanced the subtle differences in reflected light properties between chalcopyrite and cubanite allowing greater certainty in distinguishing between the minerals. However, when both chalcopyrite and cubanite were not in the same field of view, some sulfide type determinations could not be confirmed. Analysis via electron microprobe or scanning electron microscope is necessary for absolute confirmation of the sulfide mineral types.

Many of the sulfide grains observed had coatings of variable thickness. To avoid inadvertent bias of the coating measurements, two axes oriented perpendicular to one another that best represent the geometry of the grain were overlain on a grain image using the camera software. From these axes two grain lengths were measured. The coating thickness measurements were performed at the terminus of both ends of each axis. This procedure resulted in measurement of two grain lengths and four coating thicknesses for each sulfide grain.

The largest sulfide grains from the particle size samples were targeted for making coating thickness measurements. This approach was used because the largest sulfide grains in each sample are more likely

to represent true center sections through a grain. True center sections through a grain more accurately represent the actual coating thickness of a three dimensional shape. Smaller sulfide grains could represent off-center sections through larger grains which would result in two dimensional representations of coating thickness that are greater than the actual coating thickness. For spheres, this overestimating effect is relatively small except for sections very near the grain edge where coating thicknesses may be over two times greater than the actual thickness (fig. 1A). For other shapes, such as ellipsoids, apparent coating thicknesses can be variable and substantially greater than the actual thickness (fig. 1B). The majority of the variability of coating thickness measurements in this evaluation is hypothesized to result from the randomness of sectioning through the sulfide grains resulting in different two-dimensional coating thicknesses. If this is true, the thinnest coating thicknesses likely represent the more accurate measurements, whereas the thicker coatings (and associated reaction rates) are overestimates.

2.3 Theoretical Basis of Calculation

Several mineral reaction rate models have been developed that collectively encompass a variety of mineral reaction processes encountered in geochemical systems. Rimstidt (2014) provides an overview of three commonly applied mineral reaction models including the particle lifetime model (eq. 1), shrinking particle model (eq. 2), and shrinking core model (eq. 3). Conceptually, the particle lifetime and shrinking particle models characterize a surface-controlled mineral reaction in which the mineral completely dissolves, that is, all the reaction products are dissolved. The particle lifetime model calculates the extent of time for complete reaction of a mineral, whereas the shrinking particle model allows for determining the fraction of mineral reacted with time. The shrinking core model characterizes a diffusion-controlled mineral reaction where some reaction products remain or precipitate on the mineral surface accumulating overtime. The coating on the mineral surface inhibits the rate at which reactants can reach the reactive mineral surface and the rate reactants diffuse through the coating ultimately control the rate of the reaction. To apply the coating growth model for calculating the rate of a reaction the variables of diffusion rate, porosity, tortuosity and starting diameter must be known.

$$t_l = \frac{D_o}{2 \cdot k_+ \cdot V_m} \quad (\text{eq. 1})$$

t_l = particle lifetime (seconds)
 D_o = particle starting diameter (meters)
 k_+ = rate constant ($\text{mol} \cdot \text{m}^{-2} \cdot \text{sec}^{-1}$)
 V_m = molar volume ($\text{m}^3 \cdot \text{mol}^{-1}$)

$$t_{SPM} = \frac{D_o}{2 \cdot k_+ \cdot V_m} \cdot \left(1 - \left(1 - \left(1 - \frac{r^3}{r_o^3}\right)\right)^{1/3}\right) \quad (\text{eq. 2})$$

t_{SPM} = reaction time at some value r (seconds)
 r^3 = cubed particle radius at some time (meters)
 r_o^3 = cubed initial particle radius (meters)

$$t_{SCM} = \frac{v_r \cdot r_o^2}{2 \cdot D \cdot c_r \cdot V_m} \cdot \left(1 - \frac{2}{3} \alpha - (1 - \alpha)\right)^{2/3} \quad (\text{eq. 3})$$

v_r = (moles coating mineral/ moles reactant) ratio

r_0^2 = squared initial particle radius

D = diffusion coefficient through coating (m^2/sec)

c_r = concentration of reactant (mol/m^3)

α = mineral fraction reacted = $1 - \frac{r^3}{r_0^3}$

This study uses a modified version of the particle lifetime model to mathematically transform a coating thickness into a sulfide oxidation reaction rate. The primary advantage of using the particle lifetime model is the simplicity of the equation and only needing the measurement of a single parameter (i.e., coating thickness). The primary disadvantage of this method is that the particle lifetime model does not explicitly account for all the hydrogeochemical processes that may be occurring during the reaction. However, the model modifications (presented in section 2.4) result in a reaction rate measurement that incorporates all of the hydrogeochemical processes involved in the mineral reaction. This combining of multiple processes requires a distinction to be made to separate the rate measurements of this method from that of surface area-normalized reaction rates typically derived from batch or flow through reactor experiments (see section 1.9 of Brantley and Conrad, 2008). Therefore, the rates calculated by this evaluation method are referred to as apparent reaction rates. Importantly, the apparent reaction rates are specific to the geochemical system for which the reactions took place and incorporate all of the hydrogeochemical processes (e.g., diffusion rate through coating, change of rate with time and pH, etc.) over the duration the reaction occurred. By combining multiple processes into the apparent rate values, this method presents advantages over calculations accounting for only the surface reaction. First, for sulfide minerals that have relatively well defined reaction rate laws, a comparison can be made between the rate law and apparent rate values. This allows for the assessment of the magnitude of difference and identifies how much of an effect the various inhibiting or catalyzing effects may be between the experiment protocols. Second, for samples of similar composition which reacted for different experiment time periods, rates can be compared to assess if reaction rates increased or decreased with time. This comparison may allow for extracting the rate of inhibition or catalyzation with time. Third, previous authors have hypothesized that kinetic test reaction rates for sulfides may lie between rates determined for aqueous and non-aqueous environments (see Jerz and Rimstidt, 2004). Rates determined from this approach will allow qualitative assessment of which environment, aqueous or gaseous, is prevalent for kinetic tests.

The apparent sulfide oxidation rates calculated and presented in this report are estimates. The rates were calculated as an exercise to evaluate the merit of the method and determine if there is value in refining the approach to extract reaction rate data from kinetic tests and naturally weathering materials. In the conclusion section, method refinements are described that are necessary to increase the accuracy and precision. Only after implementing these improvements can a reasonable assessment be made of the representativeness of the calculated apparent rate values as true indicators of mineral reaction rates.

2.4 Rate Calculation Procedure

Sulfide oxidation rates were calculated using a spherical formulation of the particle lifetime model (see Rimstidt (2014) for a derivation of this formula). The particle lifetime model equation for a sphere (eq. 1) is a mathematical expression of the time it takes for a mineral with a specified diameter to completely

react. The particle lifetime model equation can be recast to solve for the rate constant if the mineral grain diameter, mineral molar volume, and particle lifetime parameters are known (eq. 4).

$$k_+ = \frac{D_o}{2 \cdot t_l \cdot V_m} \quad (\text{eq. 4})$$

Equation 4 is modified to allow determination of the rate constant from reaction coating thickness. The starting diameter (D_o) of the grain is recast as equal to the thickness of the coating removing the one-half factor from the equation (i.e., $D_o \div 2 = r_l$). Conceptually, this modification relates the thickness of the coating as equal to the radius of an unreacted particle (fig. 2). The particle lifetime parameter (t_l) is set to the time length of the experiment (t_{el}) instead of representing the reaction lifetime of an entire particle. In effect, the experiment lifetime represents the lifetime of a particle as if it had the radius of the measured coating. Implementing these modifications transforms equation 4 into equation 5 and the rate constant is referred to as an apparent reaction rate due to the combining of hydrogeochemical processes previously described. Liu et al. (2008) used a similar transformation of the particle lifetime model (eq. 6) to calculate the reaction rate of galena by measuring the change in diameter (ΔD) of galena crystals dissolved in a strong acid over some amount of time (Δt). The primary difference between methods is that Lui et al. (2008) had initial grain diameter measurements with no reaction product coatings, so direct measurement of the change in diameter was possible.

$$k_{\text{apparent}} = \frac{r_l}{t_{el} \cdot V_m} \quad (\text{eq. 5})$$

t_{el} = experiment lifetime (seconds)

r_l = equivalent sulfide coating thickness (meters)

k_{apparent} = apparent reaction rate ($\text{mol} \cdot \text{m}^{-2} \cdot \text{sec}^{-1}$)

V_m = molar volume ($\text{m}^3 \cdot \text{mol}^{-1}$)

$$R = \frac{\Delta D}{2 \cdot (\Delta t) \cdot V_m} \quad (\text{eq. 6})$$

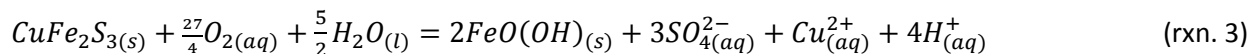
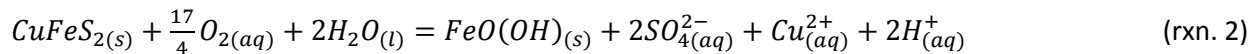
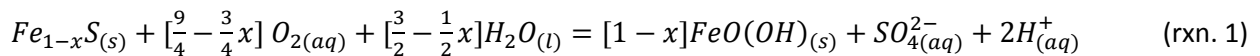
R = rate constant ($\text{mol} \cdot \text{m}^{-2} \cdot \text{sec}^{-1}$)

ΔD = change in diameter (meters)

V_m = molar volume ($\text{m}^3 \cdot \text{mol}^{-1}$)

Δt = change in time (seconds)

Because the particle lifetime model is mineral type specific (i.e., only one mineral molar volume is required) and this method measures the reaction coating not the original mineral, a transformation between the molar volumes of the reactant mineral and product mineral is required. This transformation is attained by accounting for the mineral reaction stoichiometry (rxn. 1, 2, and 3) and difference in the molar volumes between the reactant (sulfide) and product (goethite) mineral phases. For pyrrhotite and chalcopyrite oxidation reactions, the sulfide to goethite ratio is 1:1, whereas for cubanite it is 1:2.



The molar volume and reaction stoichiometry transformations are accomplished mathematically by multiplying r_l by the stoichiometric molar ratio of sulfide to goethite and the molar volume ratio of the sulfide to goethite (eq. 7). Accounting for molar volume changes results in reducing r_l for pyrrhotite, whereas r_l increases for chalcopyrite and cubanite. Microscopic observations supporting molar volume changes are presented in section 3.1 and the sensitivity of the rate calculation to the molar volume adjustment is described in section 3.2.

$$r_l = r_c \cdot \frac{\text{moles}_{\text{sulfide}}}{\text{moles}_{\text{coating}}} \cdot \frac{V_{m_{\text{sulfide}}}}{V_{m_{\text{coating}}}} \quad (\text{eq. 7})$$

r_c = average sulfide coating thickness (meters)

$V_{m_{\text{sulfide}}}$ = sulfide mineral molar volume ($\text{m}^3 \cdot \text{mol}^{-1}$)

$V_{m_{\text{coating}}}$ = coating mineral molar volume ($\text{m}^3 \cdot \text{mol}^{-1}$)

$\text{moles}_{\text{sulfide}}$ = one mole of sulfide mineral

$\text{moles}_{\text{coating}}$ = moles of goethite produced per one mole of sulfide mineral

3. RESULTS

Five polished one inch diameter grain mounts of kinetic test materials were microscopically examined. Table 1 lists the average coating thicknesses, whole grain dimensions, time period of kinetic testing, and calculated apparent reaction rates. Table 2 lists the mineral molar volumes that were used in the rate calculations. A total of 41 oxidation coating thicknesses were measured from oxidized chalcopyrite, cubanite, and pyrrhotite. Coating thicknesses ranged from 1.22 to 21.84 μm with an average thickness of 6.47 μm .

3.1 Petrography

Chalcopyrite, cubanite and pyrrhotite minerals were identified based on standard reflected light properties. Observing reflected light mineral properties on grain coatings less than 5 microns was difficult with the equipment available for this study. Because about half of the grains had coating thicknesses less than 5 microns, identification of the coating mineralogy was not possible for all samples. For the thickest coatings, reflected light optical properties indicated the coating mineral is most likely goethite. It was not discernible if all coatings were pure goethite, more advanced analysis is needed to determine if other reaction products make up the coatings. However, the reflected light properties of the thickest coatings being indicative of goethite lead to the decision to use the molar volume of goethite for the rate calculations. Of the 41 average coating measurements, six were from chalcopyrite, 34 from cubanite, and one from pyrrhotite. Two of the sulfide grains have a bimodal mineralogy, one contains chalcopyrite and cubanite and the other cubanite and pyrrhotite.

Many of the sulfide grains contained internal blebs or lineaments of oxidation, the latter commonly associated along internal fractures. These features were interpreted to indicate that the section through the grain may be far from the center and/or the grain was fractured prior to weathering. Despite these observations, no attempt was made to filter the data to extract the best candidates for calculating reaction rates. Instead all data was used to make reaction rate calculations. Inclusion of all measurements likely resulted in biasing reaction rates to artificially greater values because it was clear that some of the grains were sectioned far from the center of the whole grain. Many of the oxidation rinds exhibited fractures

and in some instances appeared to be partially detached from the sulfide grain. These rind textures are consistent with what would be expected for changes in the molar volume between reactant (sulfide) and product (goethite).

3.2 Microscope Measurements and Apparent Rate Calculations

The coating thickness measurements were performed on kinetic test samples (e.g., humidity cells) which had been in operation for 134, 1065, 1072, and 1126 weeks. The average apparent oxidation rates for samples reacting for 134 weeks are 2.20×10^{-9} , 1.17×10^{-9} , and 5.28×10^{-10} mol·m⁻²·s⁻¹ for pyrrhotite, chalcopyrite, and cubanite, respectively. The greater rate for pyrrhotite is consistent with qualitative observations made by other investigators that pyrrhotite reacts faster than chalcopyrite (see compilation by Plumlee, 1999 (table 3.4); and Jambor, 1994). The average apparent oxidation rates calculated from experiments lasting greater than 1000 weeks for chalcopyrite and cubanite were 2.75×10^{-10} and 2.76×10^{-10} mol·m⁻²·s⁻¹, respectively. These rates are a factor of 4 and 2 less than the 134 week measurements for chalcopyrite and cubanite, respectively. This rate decrease may indicate that the reaction rate was inhibited over time (e.g., via diffusion of reactants through the coating), although changing geochemical conditions (e.g., fluid pH) could be responsible for the difference as well. No pyrrhotite was observed in the samples with experiment time lengths greater than 1000 weeks. However, there were abundant grains of pure goethite which likely represent completely oxidized pyrrhotite.

Evaluating the relative rates of reaction among the three sulfide minerals can be best assessed from the bimodal sulfide grains. Because these grains have different sulfide minerals adjacent to one another, the effect of grain sectioning to apparent coating thickness is minimized, allowing more straight forward comparison between coating thickness measurements. Images of the bimodal grains show clear differences in coating thickness for the different mineral types (fig. 3A and 3B) and represent excellent candidates to directly compare reaction rates. Comparison between the rates calculated from the coating thicknesses (table 3) indicate that cubanite reacts 1.1 times faster than chalcopyrite and pyrrhotite reacts 6.1 times faster than cubanite. By multiplying these two reaction rate ratios, it can be determined that pyrrhotite reacts about 7 times faster than chalcopyrite. Because these measurements were collected from bimodal mineral grains reacting under similar conditions, they likely represent the best estimates of relative oxidation rates for these experiment conditions. These reaction rates are consistent with previous qualitative observations that pyrrhotite oxidizes faster than chalcopyrite and also indicates that the cubanite oxidation rate may be similar to chalcopyrite.

3.3 Sensitivity Analysis of the Apparent Rate Calculation

Coating thicknesses could be determined down to an accuracy of ± 0.1 microns. Samples from kinetic tests with the shortest reaction periods are more sensitive to the coating measurement accuracy because the coating thickness is related to a shorter period of time. The coating thickness measurement accuracy correlates to a maximum 17% rate error (for all sulfide types) for the experiment samples from 134 week experiments and up to a 3% rate error for the experiment samples lasting for greater than 1,000 weeks.

The molar ratio between reactant and product indicates that the molar volume transformation would reduce the calculated pyrrhotite apparent reaction rate by a factor of 0.8, and increase the chalcopyrite and cubanite apparent rates by factors of 2.1 and 1.6, respectively. These molar volume factors do not account for any porosity that may develop in the coating.

3.4 Comparison to Available Reaction Rate Data

Figure 4 illustrates the pyrite reaction rate laws of Williamson and Rimstidt (1994), pyrrhotite oxidation rate law of Chirita and Rimstidt (2014), the pyrrhotite oxidation rate data of Nicholson and Scharer (1994), and the chalcopyrite ferric iron oxidation rate law of Kimball et al. (2010). To allow equal comparison among the rate laws, the Nicholson and Scharer (1994) and Williamson and Rimstidt (1994) rates were converted from BET surface area normalized to geometric surface area normalized. The rate data from Nicholson and Scharer (1994) was converted to geometric surface area using equation 8, which was originally used by Nicholson and Scharer (1994) to transform their geometric surface areas to projected BET normalized surface areas. The Williamson and Rimstidt (1994) rate laws were adjusted appropriately using the average geometric surface areas from their study and those of the studies they used data from to derive the rate laws (table 4). The Chirita and Rimstidt (2014) and Kimball et al. (2010) rate equations were developed using geometric surface areas so no surface area transformation is necessary.

$$\log A_s = 0.415 - \log(d) \quad (\text{eq. 8})$$

A_s = specific surface area ($\text{m}^2 \cdot \text{g}^{-1}$)
 d = particle diameter (m)

The Kimball et al. (2010) rate law (eq. 9) for ferric iron oxidation of chalcopyrite includes a total ferric iron concentration parameter. Total ferric iron concentrations were calculated using Geochemist's Workbench modeling software assuming an atmospheric equilibrated water at 25 °C, saturated with respect to jarosite ($\log_{10} K = -8.89$) for pH values from 2 to 3 with charge balanced by sulfate (table 5). A fluid potassium concentration of 10 and 100 mg/kg was used to impart jarosite stability. The order of magnitude range for potassium concentration was performed to allow assessment of the sensitivity of using jarosite solubility to extract iron concentration parameters for the chalcopyrite rate model. The same approach was used for the ferric and ferrous specie molal concentration parameters needed for the Williamson and Rimstidt (1994) rate law.

$$r_{Fe^{3+}} = 10^{1.88} \times e^{-48100/RT} \times [H^+]^{0.8} \times [Fe^{3+}]^{0.42} \quad (\text{eq. 9})$$

$r_{Fe^{3+}}$ = reaction rate ($\text{mol} \cdot \text{m}^{-2} \cdot \text{sec}^{-1}$)
 R = universal gas constant ($8.314462 \text{ J} \cdot \text{mol}^{-1} \cdot \text{K}^{-1}$)
 T = temperature Kelvin (298.15 K)

Representative kinetic test pore water pH values were determined using a two-step phase. First, the average leachate pH from weekly leachate pH measurements was determined for each of the samples. Second, because the leachate pH represents a diluted flushing of the pore water reacting in the kinetic tests and the actual pore water pH would be more representative of the fluid for which reactions are occurring, a simple geochemical model was used to estimate pore water pH. The geochemical model used a representative fluid leachate composition (table 6) and reduced the fluid volume from 600 mL to 100 mL of water to scale the leachate volume down to the remnant pore volume retained by the kinetic test materials after a rinse cycle. Most humidity cell tests retain about 100 mL of water over the 1 week period between the 500 mL rinse intervals. This simple water extraction model resulted in reducing the fluid pH by about 0.7 pH units. The simple pH model approach conducted here allows a quick way to estimate a representative pore water pH. However, this approach is likely not absolutely representative of the pH. Primary factors that may influence pH that are not accounted for by the modeling approach include: (1) leachate pH trends occurring over the time period of the kinetic tests, (2) microscale chemical gradients

likely result in more acidic conditions near the oxidation boundary, (3) the small amount of alkalinity (about 0.1 mg/kg carbonate equivalent) contributed from the atmospheric equilibrated rinse water, and (4) water volume retention variations changing overtime and by sample. Despite these factors likely modifying pore water pH, the dilution from weekly rinsing of the kinetic tests appears to be the primary factor affecting pH. The 0.7 pH unit shift was applied to all of the calculated apparent reaction rates plotted on figure 4.

The single pyrrhotite apparent rate calculation is close to the trend defined by the Nicholson and Scharer (1994) data. However, more measurements are needed to determine whether or not this measurement is representative or an outlier. No clear comparisons can be made between the chalcopyrite and cubanite apparent rates and the single chalcopyrite rate law. However, the measurements do plot below the pyrite-pyrrhotite rate laws as expected. For chalcopyrite, the primary question remains as to how reactive is chalcopyrite in a mildly acidic environment where dissolved ferric iron concentrations are low. It is conceivable that the reaction mechanism for the apparent reaction rates is predominantly a function of dissolved oxygen whereas the Kimball et al. (2010) chalcopyrite rate law ($\text{pH} < 3$) is more a function of dissolved ferric iron concentration. Considering possible reaction mechanism differences and the approximately order of magnitude range in apparent rate values, more constraints on the method to reduce the uncertainty are needed.

Figure 5 shows the rate laws for ferric iron oxidation and oxygen oxidation of pyrite developed by Williamson and Rimstidt (1994) and apparent reaction rates for pyrite grains that had been naturally weathering for 2 and 3 years. The rates were calculated using eq. 3 and the pyrite oxide coating thickness measurements from Jacobs et al. (2015). The apparent rates plot well below that of the rate law. Because the samples came from a 1 to 2 foot depth, access to oxygen may be limiting, possibly explaining why the apparent rates are less than the rate law. In addition, the lower range and median apparent rates for the fine tailing may be an indication of reaction inhibition due to oxygen diffusion through the nearly saturated material or occurrence of preferential flow pathways resulting in variability of reaction rates due to different amounts of reactant (e.g., dissolved oxygen in infiltrating water). The similarity in upper bounds of both tailing types and the median value for coarse tailing of the pyrite reaction rates with the rate law defined by Williamson and Rimstidt (1994) demonstrates this rate calculation approach may closely approximate the actual rate of oxidation in natural systems near the ground surface. Further testing with a greater constraint on sample size and selection type is warranted to identify parameters and processes that may explain how natural rates compare to the laboratory experiments.

4. CONCLUSIONS

This method evaluation has shown causal importance with the techniques and mechanistic geochemistry from other sulfide oxidation rate studies. However, a considerable amount of uncertainty remains with this rate calculation technique. While conducting this evaluation many areas for improvement were identified. These improvements include: (1) using a known smaller particle size range will enable identifying grains sectioned close to their center for the most representative coating measurements, (2) a greater selection of samples from different experiments, natural settings, and rock types to assess whether or not this rate determination is sensitive to specific samples and settings, (3) evaluate samples of similar mineralogy with different pore water pH values to determine if the pore water pH effects are similar to that of available sulfide oxidation rate laws, and (4) determining whether or not coatings contain microporosity which would result in greater observed thicknesses than the actual amount of coating produced from the oxidation reaction. After making these improvements, a reasonable assessment of the

approach could be made to determine whether or not this type of rate calculation has merit for understanding the rate of sulfide oxidation in laboratory and field environments for purposes of informing the development of water quality models for mining operations.

Despite aspects for improvement of the method, this evaluation did demonstrate that direct measurement of rinds to determine sulfide oxidation rates is a viable method. Other techniques to determine surface area normalized rates from kinetic tests are limited by uncertainty in the measurements of sulfide grain size distribution, amount of sulfide grain exposure, and representative sulfide mineralogy. The general agreement between the geometric surface area normalized rates determined from batch reactor tests and those calculated from the method described in this report support using this coating thickness measurement approach for determining apparent reaction rates of sulfide minerals. The approach evaluated in this study may also have benefits over typical surface area normalized rates in that this approach directly measures the rates based on the specific hydrogeochemical conditions. Although the result of this method may not determine the rate of the elementary reaction, it does incorporate the various hydrogeochemical phenomena that are otherwise difficult to apply to surface area rates for predicting the water chemistry of mine waters.

The apparent rates calculated for the coarse pyrite median are a factor of 3.4 less than the Williamson and Rimstidt (1994) rate law and the pyrrhotite apparent rate is a factor of 1.6 less than the Scharer and Nicholson (1994) data trend. Considering these relationships, the hypothesis by Jerz and Rimstidt (2004) that kinetic test sulfide oxidation rates are between aqueous oxidation and water saturated air oxidation appears to be true. The kinetic test and field environments investigated in this study imply that the sulfide oxidation reaction proceeds at a rate more like aqueous environments than those of moist air.

In summary, evaluation of this technique has demonstrated reasonable agreement with previously reported sulfide oxidation rates. The relative ease of measurement and calculation to determine apparent sulfide oxidation rates is a promising technique for documenting the oxidation process for sulfides in mine wastes. In particular, refinement of this technique has the possibility to assess how sulfide oxidation rates may change over long periods of time. Although the contributing factors for reaction rate inhibition may not be discernible, determining whether or not there is a significant change in sulfide oxidation rates is fundamental to making long term prediction of mine waste leachate quality and can affect the associated decisions for managing mine wastes and assessing risk at mine sites.

5. ACKNOWLEDGEMENTS

The authors thank George Hudak, Steve Monson-Geerts, and John Heine for assistance and access to the Natural Resources Research Institute microscope lab for confirmation of sulfide mineralogy. This research was funded by the State of Minnesota with contribution from Mining Minnesota to the Lands and Minerals Division Cooperative Environmental Research Program.

6. REFERENCES

- Brantley, S.L.; Conrad, C.F. (2008) Analysis of rates of geochemical reactions. in: Brantley, S.L.; Kubicki, J.D.; White, A.F. (eds.), *Kinetics of Water–Rock Interaction*. Springer, New York, pp. 1–37.
- Bavin, T.; Koski, S.; Jacobs, C.; Berndt, M.; Kelly, M. (2016) Physical and hydrologic properties of taconite tailings. MN DNR report, 50 p. with appendices
- Brunauer, S; Emmett, P. H.; Teller, E. (1938). Adsorption of gases in multimolecular layers. *Journal of the American Chemical Society*, v. 60, p. 309–319.
- Chirita, P.; Rimstidt, D.J. (2014). Pyrrhotite dissolution in acidic media. *Applied Geochemistry*, v. 41, p. 1-10.
- Holmes, P.R.; Crundwell, F.K. (2000) The kinetics of the oxidation of pyrite by ferric ions and dissolved oxygen: An electrochemical study. *Geochimica et Cosmochimica Acta*, v. 64, p. 263–274.
- Jacobs, C.; Koski, S.; Bavin, T.; Berndt, M. (2015) Sulfur concentrations and pyrite textures in coarse and fine taconite tailings exposed to the elements for 0 to 30 years. MN DNR report, 88 p.
- Jambor, J.L. (1994) Mineralogy of sulfide-rich tailings and their oxidation products; in, J.L. Jambor and D.W. Blowes (eds.), *Short Course on Environmental Geochemistry of Sulfide-Mine Wastes*. Mineralogical Association of Canada Short Course Handbook. v.22, p. 59-102.
- Kimball, B.E.; Rimstidt, J.D.; Brantley, S.L. (2010) Chalcopyrite dissolution rate laws. *Applied Geochemistry*, v. 25, p. 972–983.
- Lapakko, K. (1999) Laboratory drainage quality from Duluth Complex rock and assessment of test methods for waste rock dissolution. MN DNR report on contract BLM J910C82009. Delivered to U.S. Bureau of Land Management Salt Lake City, 32 p. plus appendices.
- Lapakko, K.A.; Engstrom, J.N.; Antonson, D.A. (2006) Effects of particle size on drainage quality from three lithologies. 7th ICARD proceedings, St. Louis, MO USA. 33 p.
- Liu, J., Aruguete, D.M., Jinschek, J.R., Rimstidt, J.D., and Hochella Jr., M.F. (2008). The non-oxidative dissolution of galena nanocrystals: Insights into mineral dissolution rates as a function of grain size, shape, and aggregation state. *Geochimica et Cosmochimica Acta*, v. 72, p. 5984-5996.
- McKibben, M.A.; Barnes, H.L. (1986) Oxidation of pyrite in low temperature acidic solutions: rate laws and surface textures. *Geochimica et Cosmochimica Acta*, v. 50, p. 1509-1520.
- Moses, C.O.; Herman, J.S. (1991) Pyrite oxidation at circumneutral pH. *Geochimica et Cosmochimica Acta*, v. 55, p. 471–482.

Nicholson, R.V. (1994) Iron-sulfide oxidation mechanisms: Laboratory studies; in, J.L. Jambor and D.W. Blowes (eds.), Short Course on Environmental Geochemistry of Sulfide-Mine Wastes. Mineralogical Association of Canada Short Course Handbook. v.22, p. 163-183.

Nicholson, R. V.; Scharer J. M. (1994) Laboratory studies of pyrrhotite oxidation kinetics. In Environmental Geochemistry of Sulfide Oxidation (ed. C. N. Alpers and D. W. Blowes), pp. 14–30. American Chemistry Society, Washington D.C.

Parks, G.A. (1990) Surface energy and adsorption at mineral-water interfaces: An introduction. Reviews in Mineralogy, v.23, p. 133-175.

Plumlee, G.S. (1999) The environmental geochemistry of mineral deposits; in G. S. Plumlee and M.J. Logsdon (eds.), The Environmental Geochemistry of Mineral Deposits. Review in Economic Geology, v. 6A, p. 71-116.

Rimstidt, J.D. (2014) Geochemical Rate Models. Cambridge University Press, United Kingdom. 232 p.
Tester, J.W.; Worley, G.; Robinson, B.A.; Grisby, C.O.; Feerer, J.L. (1994) Correlating quartz dissolution kinetics in pure water from 25 to 625 °C. Geochimica et Cosmochimica Acta, v. 58, p. 2407–2420.

Tester, J.W., Worley, G., Robinson, B.A., Grisby, C.O., Feerer, J.L. (1994) Correlating quartz dissolution kinetics in pure water from 25 to 625 °C. Geochimica et Cosmochimica Acta v. 58, p. 2407–2420.

Wenz, Z.J.; Lapakko, K.; Antonson, D. (2013) Rock composition, leachate quality and solute release as a function of particle size for three waste rock types: An 18 year laboratory experiment. MN DNR report, 125 p. with appendices.

Williamson, M.A.; Rimstidt, J.D. (1994) The kinetics and electrochemical rate determining step of aqueous pyrite oxidation. Geochimica et Cosmochimica Acta, v. 58, p. 5443-5454.

TABLES

Table 1. Sulfide grain coating average thickness measurements and corresponding apparent reaction rates. Sample ID's starting with PS are from the 'particle size experiment' (Wenz et al., 2013) and samples starting with M are from the 'BLM experiment' (Lapakko, 1999).

Sample ID	grain ID#	Mineral	Average pH	grain length (um)	grain width (um)	r_c (um)	r_c (m)	r_l (m)	time (wks)	t_{el} (s)	$k_{apparent}$ (mol·m ⁻² ·sec ⁻¹)
PS14	P14_3	chalcopyrite	5.4	83.16	13.99	2.2	2.2E-06	4.7E-06	1065	644,112,000	1.65E-10
PS14	P14_6	chalcopyrite	5.4	53.8	42.25	2.6	2.6E-06	5.5E-06	1065	644,112,000	1.93E-10
PS14	P14_8	chalcopyrite	5.4	31.5	26.17	2.2	2.2E-06	4.6E-06	1065	644,112,000	1.62E-10
PS16	PS16_1.1	chalcopyrite	5.1			3.4	3.4E-06	7.2E-06	1126	681,004,800	2.39E-10
PS16	PS16_6	chalcopyrite	5.1	266.8	225.9	8.8	8.8E-06	1.8E-05	1126	681,004,800	6.17E-10
PS17	PS17_1	chalcopyrite	5.6	145.7	144.3	2.0	2.0E-06	4.2E-06	134	81,043,200	1.17E-09
PS14	P14_1	cubanite	5.4	49.24	33.13	6.1	6.1E-06	9.8E-06	1065	644,112,000	2.26E-10
PS14	P14_2	cubanite	5.4	27.21	15.98	6.7	6.7E-06	1.1E-05	1065	644,112,000	2.50E-10
PS14	P14_4	cubanite	5.4	49.46	32.54	5.4	5.4E-06	8.7E-06	1065	644,112,000	2.00E-10
PS14	P14_5	cubanite	5.4	39.4	17.46	5.3	5.3E-06	8.6E-06	1065	644,112,000	1.99E-10
PS14	P14_7	cubanite	5.4	25.21	11.81	2.8	2.8E-06	4.6E-06	1065	644,112,000	1.05E-10
PS14	P14_9	cubanite	5.4	33.08	19.26	7.4	7.4E-06	1.2E-05	1065	644,112,000	2.76E-10
PS14	P14_10	cubanite	5.4	35.69	28.07	3.0	3.0E-06	4.9E-06	1065	644,112,000	1.13E-10
PS15	PS15_1	cubanite	5.3	97.43	60.33	21.8	2.2E-05	3.5E-05	1065	644,112,000	8.13E-10
PS15	PS15_2	cubanite	5.3	85.08	40.15	9.9	9.9E-06	1.6E-05	1065	644,112,000	3.69E-10
PS15	PS15_3	cubanite	5.3	78.29	33.5	8.4	8.4E-06	1.4E-05	1065	644,112,000	3.13E-10
PS15	PS15_4	cubanite	5.3	170.7	91.57	20.8	2.1E-05	3.4E-05	1065	644,112,000	7.74E-10
PS15	PS15_5	cubanite	5.3	101.2	36.09	5.8	5.8E-06	9.4E-06	1065	644,112,000	2.17E-10
PS16	PS16_1	cubanite	5.1			7.8	7.8E-06	1.3E-05	1126	681,004,800	2.73E-10
PS16	PS16_2	cubanite	5.1	164.7	148.2	12.0	1.2E-05	1.9E-05	1126	681,004,800	4.23E-10
PS16	PS16_3	cubanite	5.1	233.6	164.7	4.9	4.9E-06	7.9E-06	1126	681,004,800	1.72E-10
PS16	PS16_4	cubanite	5.1	334.9	114.9	7.7	7.7E-06	1.2E-05	1126	681,004,800	2.71E-10
PS16	PS16_5	cubanite	5.1	242	195.7	11.0	1.1E-05	1.8E-05	1126	681,004,800	3.88E-10
PS16	PS16_7	cubanite	5.1	72.31	60.25	7.7	7.7E-06	1.2E-05	1126	681,004,800	2.71E-10
PS16	PS16_8	cubanite	5.1	258.5	94.17	3.5	3.5E-06	5.6E-06	1126	681,004,800	1.22E-10
PS16	PS16_9	cubanite	5.1	269.7	205.5	4.5	4.5E-06	7.2E-06	1126	681,004,800	1.57E-10
PS16	PS16_10	cubanite	5.1	346.4	163.6	15.7	1.6E-05	2.5E-05	1126	681,004,800	5.53E-10
PS16	PS16_11	cubanite	5.1	132.6	66.22	4.1	4.1E-06	6.7E-06	1126	681,004,800	1.45E-10
PS17	PS17_2	cubanite	5.6	362.6	304.8	1.4	1.4E-06	2.3E-06	134	81,043,200	4.26E-10
PS17	PS17_3	cubanite	5.6	154	80.01	2.7	2.7E-06	4.3E-06	134	81,043,200	7.96E-10
PS17	PS17_6.1	cubanite	5.6			1.2	1.2E-06	2.0E-06	134	81,043,200	3.62E-10
M21	M22_1	cubanite	4.8	880.6	605.9	6.5	6.5E-06	1.1E-05	1072	648,345,600	2.41E-10
M22	M22_2	cubanite	4.8	103.1	28.18	2.1	2.1E-06	3.4E-06	1072	648,345,600	7.73E-11
M22	M22_3	cubanite	4.8	80	65.99	3.5	3.5E-06	5.6E-06	1072	648,345,600	1.28E-10
M22	M22_4	cubanite	4.8	106.1	61.56	3.6	3.6E-06	5.9E-06	1072	648,345,600	1.34E-10
M22	M22_5	cubanite	4.8	221.6	80.72	7.5	7.5E-06	1.2E-05	1072	648,345,600	2.79E-10
M22	M22_6	cubanite	4.8	53.75	34.25	3.4	3.4E-06	5.5E-06	1072	648,345,600	1.25E-10
M22	M22_7	cubanite	4.8	78.89	52.17	4.0	4.0E-06	6.5E-06	1072	648,345,600	1.49E-10
M23	M22_8	cubanite	4.8	79.68	55.41	9.3	9.3E-06	1.5E-05	1072	648,345,600	3.45E-10
M22	M22_9	cubanite	4.8	282.4	252.9	12.2	1.2E-05	2.0E-05	1072	648,345,600	4.53E-10
PS17	PS17_6	pyrrhotite	5.6			3.7	3.7E-06	3.1E-06	134	81,043,200	2.20E-09

Table 2. Mineral molar volumes

Mineral	cm ³ /mol	m ³ /mol
goethite	20.84	2.08E-05
pyrite	23.9	2.39E-05
pyrrhotite	17.43	1.74E-05
chalcopyrite	43.91	4.39E-05
cubanite	67.46	6.75E-05

Table 3 Bimodal sulfide grains with associated apparent reaction rates. Ratios of the rates from each bimodal grain illustrate the difference in reaction rate among the different sulfides.

Grain	Mineral	r_c (um)	r_l (m)	time (wks)	t_{el} (s)	$k_{apparent}$ (mol·m ⁻² ·sec ⁻¹)	cub/cpy	po/cub	po/cpy
PS16_1.1	chalcopyrite	3.4	7.16E-06	1126	681004800	2.39E-10			
PS16_1	cubanite	7.76	1.26E-05	1126	681004800	2.73E-10	1.1		
PS17_6	pyrrhotite	3.71	3.10E-06	134	81043200	2.20E-09			
PS17_6.1	cubanite	1.22	1.98E-06	134	81043200	3.62E-10		6.1	
									6.9

Table 4. BET and geometric surface area conversion data

Source	Primary oxidant for rate law	grain size (um)	SSA _{BET} (m ² ·g ⁻¹)	D _e (um)	D _e (m)	SSA _{geo} (m ² ·g ⁻¹)	SSA _{BET} /SSA _{geo}	
Williamson and Rimstidt (1994)	Fe ³⁺	150-250	0.047	196	1.96E-04	0.0061	7.7	
McKibben (1984)	Fe ³⁺	125-250	0.0251	180	1.80E-04	0.0066	3.79	
Smith (1970)	Fe ³⁺	105-250	0.12	167	1.67E-04	0.0072	16.78	9.42
McKibben and Barnes (1986)	O ₂	125-250	0.0251	180	1.80E-04	0.0066	3.79	
Moses and Herman (1991)	O ₂	38-45	0.0709	41	4.14E-05	0.0289	2.46	

Source	Primary oxidant for rate law	grain size (um)	SSA _{BET} (m ² ·g ⁻¹)	D _e (um)	D _e (m)	SSA _{geo} (m ² ·g ⁻¹)	SSA _{BET} /SSA _{geo}	
Smith et al. (1970)	O ₂	105-250	0.12	167	1.67E-04	0.0072	16.78	
							average	7.67

D_e=effective diameter using the averaging method of Tester et al. (1994).

Table 5. Ferric iron geochemical model input and output data.

pH	K (mg/kg)	SO ₄ ⁻⁻ (mg/kg)	m _{Fe⁺⁺}	m _{FeSO₄⁺}	m _{FeOH⁺⁺}	m _{Fe(OH)₂⁺}	m _{Fe⁺⁺⁺}	m _{Fe(SO₄)₂⁻}	m _{Fe(OH)₃}	m _{Fe₂(OH)₂⁺⁺⁺⁺}	m _{Fe₃(OH)₄⁺⁺⁺⁺}	m _{FeHSO₄⁺}	m _{totalFe⁺⁺⁺}
2	10	1420	3.55E-10	4.11E-03	9.20E-05	1.99E-06	2.44E-04	2.64E-04	7.69E-11	4.61E-07	4.69E-10	2.46E-05	4.74E-03
2.5	10	246	1.63E-10	2.72E-04	4.17E-05	3.44E-06	2.88E-05	6.70E-06	4.48E-10	7.66E-08	9.59E-11	4.27E-07	3.53E-04
3	10	71	8.16E-11	1.94E-05	2.07E-05	5.93E-06	4.02E-06	1.97E-07	2.52E-09	1.62E-08	2.88E-11	8.77E-09	5.03E-05
3.5	10	30.1	3.90E-11	1.49E-06	9.89E-06	9.36E-06	5.67E-07	7.38E-09	1.28E-08	3.35E-09	8.44E-12	2.04E-10	2.13E-05
4	10	18.3	1.61E-11	1.27E-07	4.08E-06	1.25E-05	7.17E-08	4.04E-10	5.43E-08	5.45E-10	1.74E-12	5.38E-12	1.68E-05
4.5	10	14.7	5.75E-12	1.18E-08	1.46E-06	1.42E-05	8.01E-09	3.07E-11	1.97E-07	6.85E-11			1.59E-05
2	100	1160	1.65E-10	1.89E-03	4.26E-05	9.31E-07	1.12E-04	1.20E-04		9.82E-08		1.12E-05	2.18E-03
2.5	100	344	6.42E-11	1.45E-04	1.64E-05	1.29E-06	1.20E-05	5.06E-06		1.27E-08		2.38E-07	1.80E-04
3	100	184	2.41E-11	1.24E-05	6.14E-06	1.62E-06	1.32E-06	2.97E-07					2.18E-05
3.5	100	141	8.29E-12	1.16E-06	2.11E-06	1.80E-06	1.40E-07	2.32E-08					5.24E-06
4	100	129	2.71E-12	1.13E-07	6.91E-07	1.88E-06	1.43E-08	2.12E-09					2.69E-06
4.5	100	125	8.67E-13	1.12E-08	2.21E-07	1.90E-06	1.44E-09		2.52E-08				2.16E-06

Table 6. Pore water pH geochemical model.

Parameter	Starting Value	Ending Value	Units
water	0.6	0.0987	kg
pH	5	4.264	s.u.
sulfate	balance	120	mg/kg
calcium	4	24	mg/kg
magnesium	1	6	mg/kg
sodium	0.5	3	mg/kg
potassium	1	6	mg/kg
nickel	2	12	mg/kg
copper	0.5	3	mg/kg
temperature	25	25	°C

FIGURES

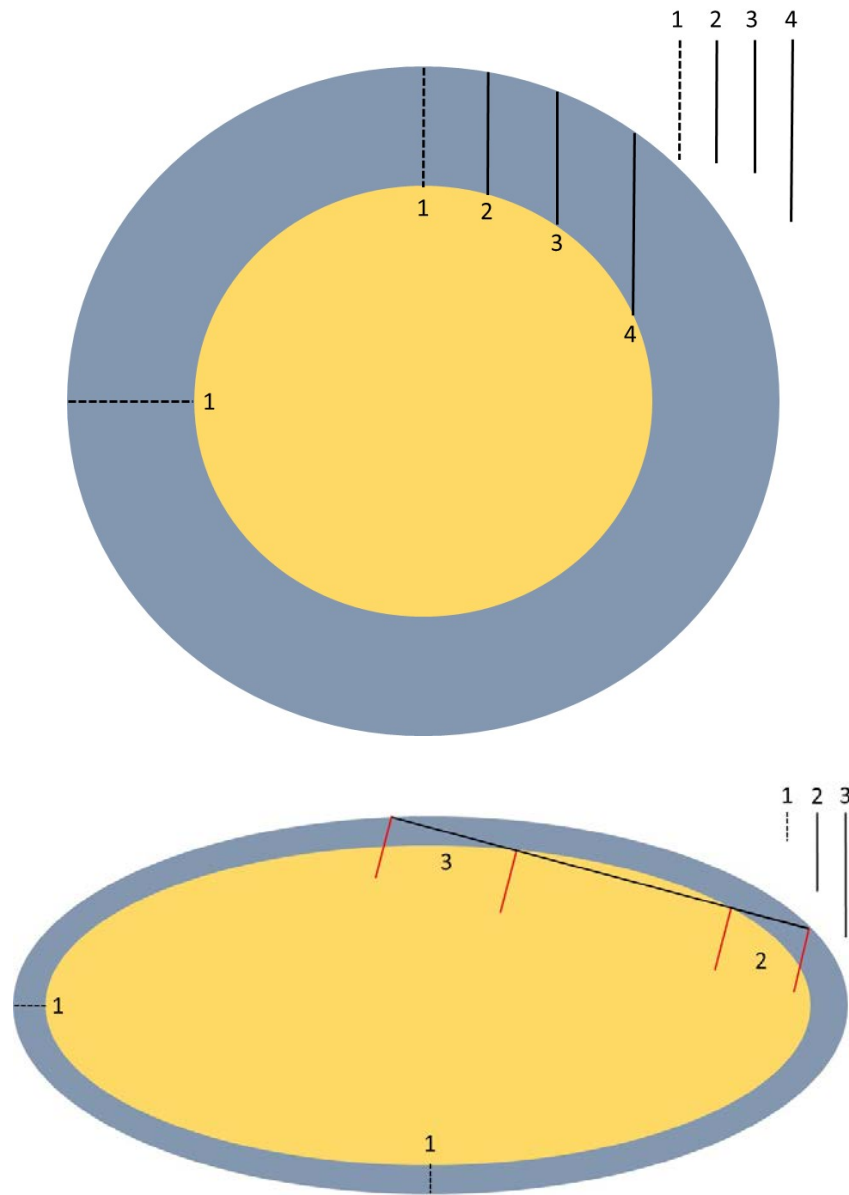
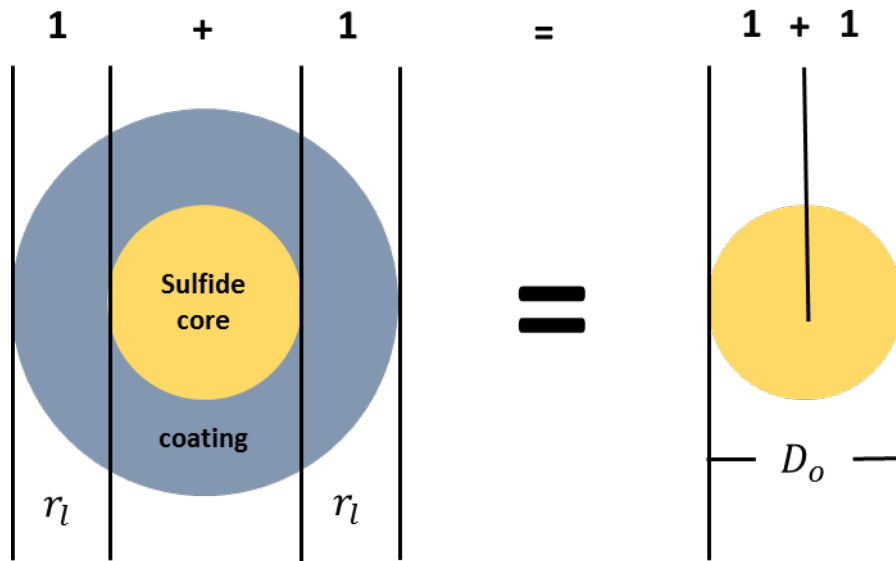
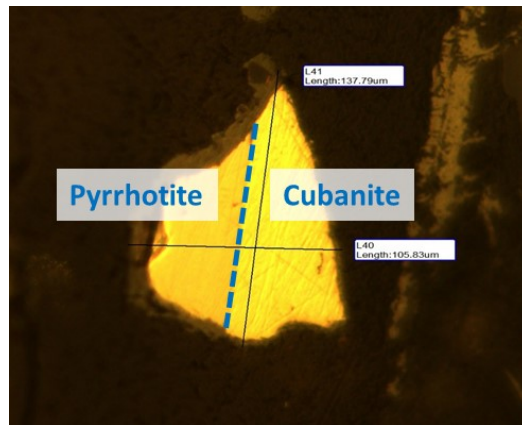
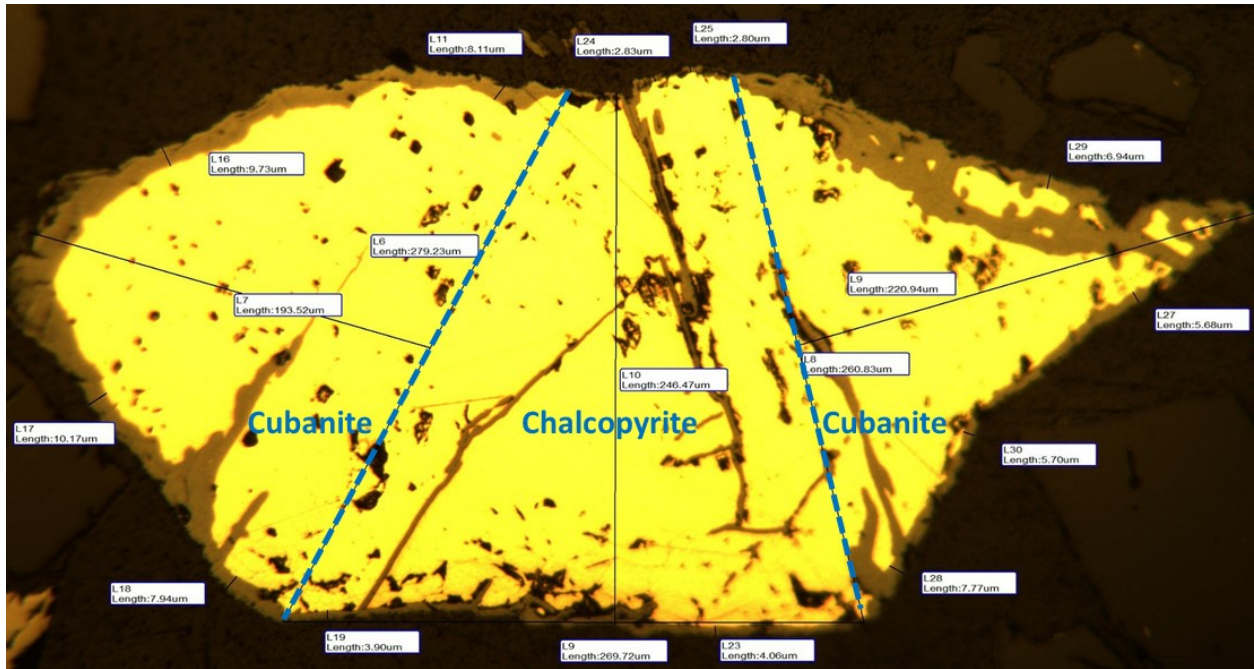


Figure 1. Illustration of cross-sections through the center of a sulfide grain with a uniform oxidation reaction product coating. Numbered segments in these cross-sections represent different coating thicknesses that would be viewed in a mount or thin section if the grain was sectioned at that location. Figure 1A illustrates the apparent coating thickness for a uniformly reacted sphere increasing from the center towards the edge. Figure 1B illustrates the apparent coating thickness for an oblique section through an ellipsoid. This demonstrates how coating thickness in a cross section could overestimate the actual thickness by over a factor of four.



$$r_l = D_o \div 2$$

Figure 2. Schematic illustrating the relationship between coating thickness from measured grains and the particle lifetime conceptualized counterpart. The image on the left shows a partially reacted sulfide grain where the unreacted core is orange and the reaction product coating is blue whereas the image on the right shows a completely reacted sulfide grain. The image on the left is a schematic of what the sulfide grains look like in an idealized spherical geometry indicating a uniform coating with a thickness of 1. The image on the right depicts a completely oxidized sulfide grain that has the same reaction coating as the partially reacted grain (left image) visually demonstrating that the coating radius is equivalent in both images and the resulting age calculated from the particle lifetime model would likewise be equal.



Figures 3A and 3B. Figures 3A and 3B are images of the two bimodal sulfide mineral grains observed. The dashed blue lines represent the mineral grain boundaries identified using reflected light microscopy. The oxidation reaction product coating is gray and encompasses all of the sulfide surface. In 3A the cubanite has visibly greater coating thickness. In 3B, the pyrrhotite half of the grain has a noticeably greater thickness coating.

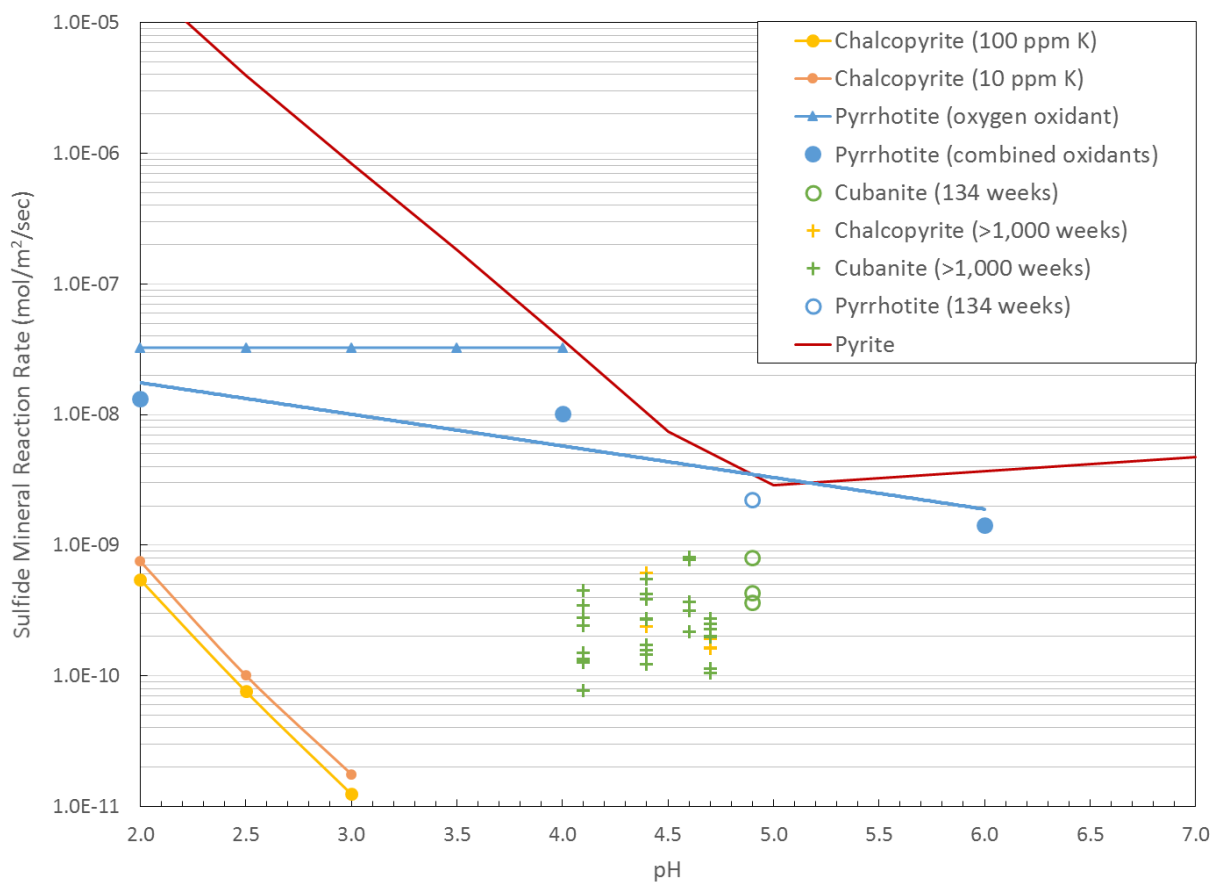


Figure 4. Sulfide mineral oxidation rate plot illustrating chalcopyrite and pyrrhotite rate laws and rate data. Open circles and crosses represent apparent rates for the 134 week and greater than 1,000 weeks samples used in this study. The pH values used to plot the apparent rates represent the averages of the weekly leachate pH from each sample. The pyrite rate laws shown are only for the 10 mg/kg potassium concentration geochemical model.

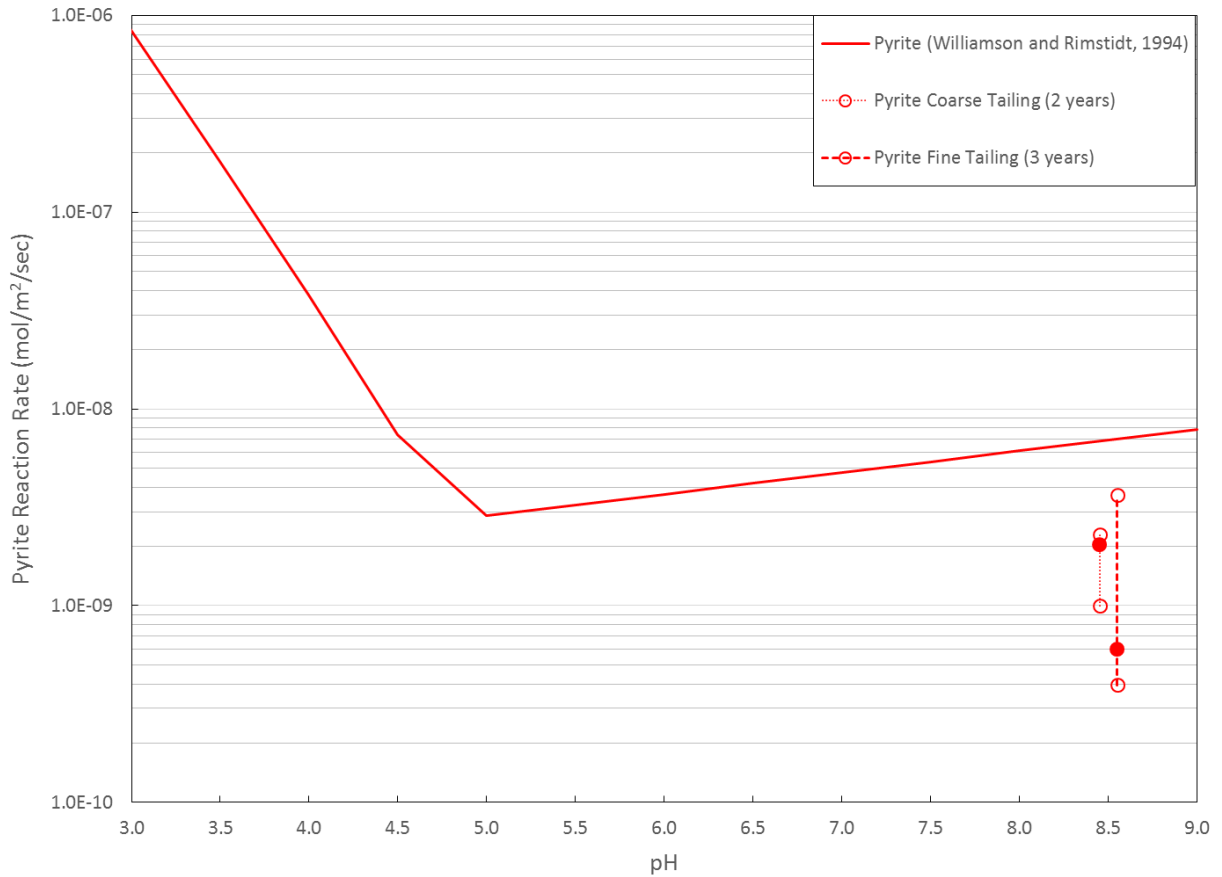


Figure 5. Pyrite oxidation rate laws from Williamson and Rimstidt (1994) illustrating the change in pyrite oxidation rate with pH and oxidant type. The dashed lines represent the range of oxidation rates for pyrite from Minnesota taconite tailing basins from coarse and fine tailing samples from the coating thickness measurements listed in Jacobs et al. (2015). The filled circles for dashed lines represent median coating thickness. Pore water pH of the tailing basin was approximately 8.5 (see Bavin et al. (2016)) and was plotted on the figure as 8.45 and 8.55 for a clearer presentation of the two tailing types reaction rate ranges.